Structure Evolution and Kinetics of Thermoreversible Gelation in a Rigid-Rod Polyimide/*m*-Cresol System

Thein Kyu,*,† Jen-Chang Yang,† Stephen Z. D. Cheng,‡ Steven L. C. Hsu,‡ and Frank W. Harris‡

Institute of Polymer Engineering and M. Morton Institute of Polymer Science, The University of Akron, Akron, Ohio 44325

Received April 5, 1993; Revised Manuscript Received December 28, 1993•

ABSTRACT: Biphenyltetracarboxylic dianhydride–(perfluoromethyl)benzidine (BPDA–PFMB) polyimide/*m*-cresol solutions showed thermoreversible gelation associated with thermally induced phase separation and subsequent liquid crystal formation. In this study, phase equilibria and structure evolution in a BPDA–PFMB/*m*-cresol solution were investigated by differential scanning calorimetry, polarized optical microscopy, and depolarized light scattering. A temperature–composition phase diagram of BPDA–PFMB/*m*-cresol was established by a cloud point method. Kinetic aspects of the phase transition were studied in the framework of a nucleation and growth theory. The average domain size, which characterized the length scale of rigid-rod aggregates, was found to depend on supercooling.

Introduction

It has been generally known that a number of rodlike polymer/solvent systems exhibit thermoreversible gelation associated with phase separation and/or a mesophase transition.[1-9] A chimney type phase diagram, i.e., a narrow immiscibility gap overlapping with an upper critical solution temperature (UCST), often known as the idealized Flory temperature–composition phase diagram, was predicted for rigid polymer solutions.[7] Such a phase diagram was found experimentally in a poly(γ-benzyl L-glutamate) (PBLG)/dimethylformamide (DMF) system.[2-4] Newer theories of concentration fluctuations and phase separation of rigid-rod solutions were put forth by Doi et al.[8] by including the orientational order parameter of liquid crystals. Recently, Russo and co-workers[4] pursued the dynamics of phase separation by time-resolved video microscopy on a PBLG/DMF system having traces of water. The analysis of the structure factor, as determined by the Fourier transform of video images, showed a kinetic exponent of $^1/_3$, in conformity with the evaporation–condensation model.

An inverted phase diagram, i.e., a funnel type phase diagram in which a narrow immiscibility gap overlapped with a lower critical solution temperature (LCST), was also predicted for a rodlike macromolecular solution. The effect of chain flexibility and aspect ratio of rodlike molecules was incorporated in the theory.[9] Such a phase diagram was observed experimentally for a hydroxypropyl cellulose (HPC)/water system.[6] At low concentrations of HPC, thermally induced phase separation occurred while a cholesteric liquid crystal phase was observed at ~60 wt % polymer concentration. At ~70 wt %, the system exhibited thermoreversible gelation. Beyond 90 wt %, a solid film was formed. The kinetics of phase separation by spinodal decomposition (SD) was reported for low HPC contents in which the time evolution of the structure factor was analyzed in the context of the linearized Cahn–Hilliard theory for the early stage of SD and the Siggia theory for the late stages of SD where hydrodynamic flow takes place.[6]

The formation of a liquid crystal mesophase was recognized recently in organosoluble aromatic rigid-rod polyimide/*m*-cresol systems.[10] These polyimides were synthesized originally for producing high-modulus and high-strength fibers, films, and molecular composites.[11] Among them, biphenyltetracarboxylic dianhydride–(perfluoromethyl)benzidine (BPDA–PFMB) is a typical polyimide which can be solution-spun to produce high-performance fibers for composite applications.[11,12] During that time, we realized that spinning from a gel state yields better spinnability and strong fibers. Such a behavior was also reported for ultrahigh molecular weight polyethylene (UHMWPE)/decalin gels in which gel-spinning at the gelation point yields fibers with high orientation and outstanding mechanical properties.[13-15] Therefore, the understanding of sol–gel transitions is of crucial importance for determining a processing window of polymer/solvent systems.

The purpose of the present study is to elucidate the mechanisms of mesophase transitions associated with thermoreversible gelations of the rigid-rod BPDA–PFMB/*m*-cresol system. In a previous paper,[16] the effects of molecular weight and concentration on the sol–gel transitions of BPDA–PFMB/*m*-cresol solution were investigated. Now, we focus our attention on the establishment of the phase diagram and the determination of the kinetics of the phase transformation involving mesophase transitions.

Experimental Section

Materials. The synthesis and characterization of BPDA–PFMB were reported elsewhere.[10] The BPDA and PFMB monomers were first dissolved in *m*-cresol and then polymerized. The concentration of BPDA–PFMB thus produced was ~10 wt %. The inherent viscosity of BPDA–PFMB was measured with an Ubbelohde viscometer; it was estimated to be 4.7 dL/g at 30 °C. Reagent grade *m*-cresol was used to further dilute BPDA–PFMB to the desired concentrations at elevated temperatures (80 °C). The BPDA–PFMB/*m*-cresol solutions were sealed in Vitro dynamic cells for light scattering experiments.

Methods. Thermal analysis of BPDA–PFMB/*m*-cresol solutions was carried out by DSC at a heating rate of 10 °C/min under flowing nitrogen. Liquid DSC cells were utilized to ensure the mixture was sealed completely. The phase morphology of the BPDA–PFMB/*m*-cresol solutions was examined by a Leitz optical microscope (Model Laborlux 12 Pol). The kinetics of phase transition was pursued by means of time-resolved small-angle light scattering. The scattering setup consists of a He–Ne laser light source (2 mW, Aerotech), a one-dimensional Reticon diode array detector (EG&G) interlinked with an optical mul-

* To whom correspondence should be addressed.
† Institute of Polymer Engineering.
‡ M. Morton Institute of Polymer Science.
• Abstract published in *Advance ACS Abstracts*, February 15, 1994.

0024-9297/94/2227-1861$04.50/0

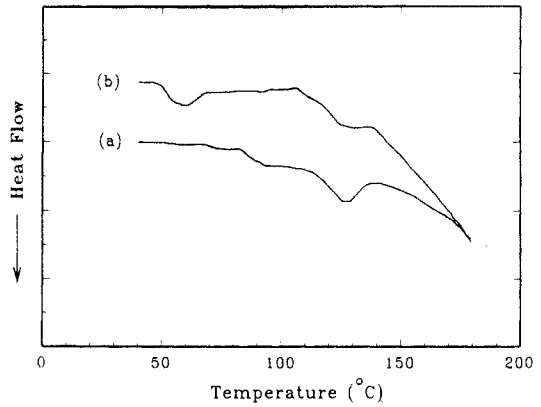

Figure 1. DSC traces for (a) a fresh sample of the 8 wt % BPDA–PFMB/*m*-cresol solution and (b) rerun of the specimen kept at room temperature for 24 h after the first run. The heating rate was 10 °C/min.

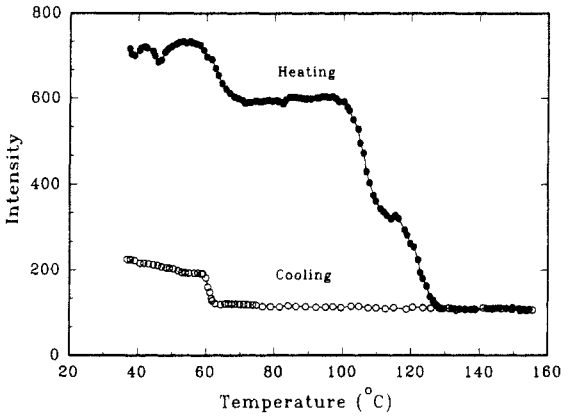

Figure 2. Temperature dependence of scattered intensity for the 8 wt % BPDA–PFMB/*m*-cresol solution with a ramp rate of 0.5 °C/min for heating and cooling.

tichannel analyzer (OMA III, EG&G), and an off-line microcomputer (IBM PC2/30). Depolarized light scattering pictures were taken on a Polaroid instant camera (Land film holder, Model 545).

Results and Discussion

Phase Equilibrium. Figure 1 shows DSC traces of a fresh 8 wt % BPDA–PFMB/*m*-cresol solution obtained during heating from 25 to 180 °C at a rate of 10 °C/min. Dual endothermic melting peaks (around 95 and 124 °C) are evident in the heating run. The specimen was rapidly quenched to room temperature and then reheated subsequently to 180 °C. The DSC trace of the second heating cycle reveals a flat base line without any indication of a transition peak (not shown here). This kind of thermal behavior is strikingly similar to that reported for poly(vinyl chloride)/diethyl malonate gels.[17] When the measurement was repeated with the sample kept at room temperature for ~24 h, the DSC trace showed two endothermic peaks corresponding to 60 and 124 °C (Figure 1). Although the higher temperature peak was reproducible in repeated heating cycles, the lower endotherm was strongly dependent on thermal history and aging time.

Figure 2 shows the temperature dependence of the scattered intensity of the fresh 8 wt % BPDA–PFMB/*m*-cresol solution with a ramp rate of 0.5 °C/min for both heating and cooling. In the heating cycle, the scattered intensity (at a scattering angle of 20°) vs temperature curve exhibits multiple transitions in the temperature range 50–140 °C. The lowest transition appears around 50–60 °C. The intensity remains constant with further increase of temperature, but it begins to drop around 100 °C. At ~112 °C, the intensity increases slightly, showing a hump

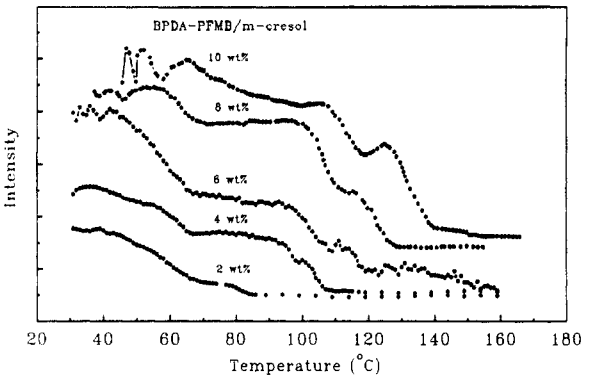

Figure 3. Change of scattered intensity as a function of ascending temperature for various BPDA–PFMB/*m*-cresol solutions. The heating rate was 0.5 °C/min.

in the intensity vs temperature curve. The increased fluidity of the sample is also noticed visually at that temperature. Then the intensity continues to decrease and disappears completely at ~129 °C as the solution reaches the isotropic state.

When the sample is cooled gradually from the isotropic state, the scattered intensity remains constant initially, but it increases rapidly at ~60 °C. However, when the system is cooled just below the highest transition temperature (e.g., 115 °C) and held at that temperature for ~2 h, a large biphasic structure is discerned in the microscopic investigation. The light scattering experiment probably missed this transition because of the fast cooling rate and the slow kinetics of the phase transitions. We therefore focus on the phase transitions of the heating runs.

To illustrate the overall phase behavior of the BPDA–PFMB/*m*-cresol system, the SALS experiment was undertaken on other compositions ranging from 2 to 10 wt % BPDA–PFMB. All specimens were preheated once to 180 °C for 5 min, cooled at a natural cooling rate, and then kept at ambient temperature for at least 1 week to ensure all specimens received the same thermal history. As shown in Figure 3, two transitions appear in the intensity vs temperature curves for the 2 wt % concentration. The first transition in the order of ascending temperature appears around 50 °C for the 2 wt % solution. This transition remains fairly constant with increasing concentration. The depolarized Hv (horizontal polarizer with vertical analyzer) light scattering studies of the 8 wt % BPDA–PFMB/*m*-cresol solution showed no change in shape or size of the four-lobe pattern during heating above 60 °C, except that the scattering intensity was reduced sharply. This suggests that the polyimide rod aggregates melt and transform to an anisotropic liquid crystal mesophase. This anisotropic structure persists up to 110 °C until gel melting takes place. This temperature incidentally corresponds to the inflection point of the intensity vs temperature curve of the 8 wt % solution in Figure 3.

The high-temperature transition virtually splits into dual transitions at 8 and 10 wt % polyimide concentrations in that the intensity seems to decrease and then increase again. In this temperature range, it was noticed visually that the gel gained fluidity; it is not uncommon for gels very near their melting point to exhibit this kind of behavior. The increased intensity may be caused by drift of laser speckle patterns as the gels undergo constant rearrangements near their melting transition. The inflection point of the intensity vs temperature curve has been taken as the gel melting temperature, which displays a strong dependence on concentration of BPDA–PFMB/*m*-cresol (Figure 3). It should be pointed out that there

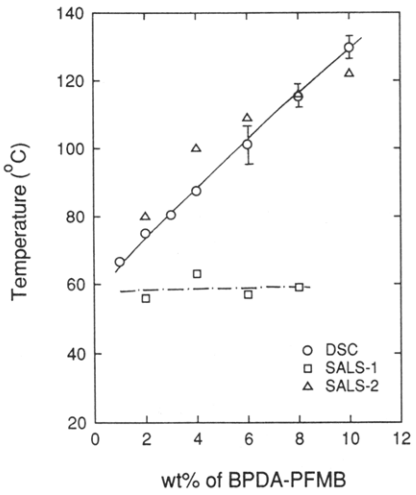

Figure 4. Temperature vs composition phase diagram of BPDA–PFMB/*m*-cresol solution based on DSC and cloud point measurements.

is considerable scattering remaining in the Vv configuration in the temperature range 110–130 °C. Although such a phenomenon has been attributed customarily to the slow gel melting process, other mechanisms such as liquid–liquid phase separation cannot be ruled out for this polyimide/*m*-cresol system since a large biphase structure can be discerned under the microscope after 2 h following a *T* quench from 180 to 115 °C. Moreover, the existence of liquid–liquid phase separation above the gel melting temperature had been reported in some flexible polymer/solvent systems.[18,19] One notable example is the observation of spinodal decomposition above the sol–gel transition of a poly(vinyl alcohol)/water system.[18] Recently, the interplay of the liquid–liquid (L–L) phase separation and sol–gel transition has been reported for a flexible coil/solvent system.[19] In the present system, we are unable to determine the L–L phase separation temperature exactly because of the strong interference of the slow gel melting process.

Based on the experimental observations by optical microscopy, DSC, and SALS measurements, a temperature–composition phase diagram was established (Figure 4). The endothermic transition peak of BPDA–PFMB/*m*-cresol solution increased from 80 to 130 °C with increasing polymer concentration from 2 to 10 wt %. The DSC gel melting points approximately correspond to the second transition as seen by light scattering. Upon cooling from a single phase into the miscibility gap, liquid–liquid phase separation probably occurs initially. The local concentration of rigid-rod polyimides increases progressively, leading to alignment or self-association of anisotropic rods due to the entropic effect. The molecular mobility would be reduced considerably, eventually causing apparent gelation. At this stage, a birefringent structure may be discerned under the polarized optical microscope. With continued cooling to ambient temperature, the rigid-rod concentration probably exceeds a certain critical concentration, thereby causing the system to lock-up or solidify as the ordered rod aggregates approach their glassy state.

The lowest transition, which appears at ~60 °C in the cloud point measurements, can be recognized in the DSC heating cycles (Figure 1). However, the exothermic peak appears at a lower temperature of ~40 °C. Such discrepancy between the melting and crystallization temperatures has been commonly observed in semicrystalline polymers, particularly for fast heating and cooling rates. This transition may be regarded as a monotectic transition from a liquid + nematic liquid phase to a liquid + solid (ordered rod aggregates) phase within the miscibility gap.

Structure Evolution in BPDA–PFMB/*m*-Cresol Solution. To ensure complete homogenization and to remove possible memory effects, the BPDA–PFMB/*m*-cresol solutions were kept at 180 °C for 90 s and then quenched into a miscibility gap close to the monotectic transition region. The optical micrographs of Figure 5 show the time evolution of phase-separated structures following a temperature (*T*) quench to 23 °C. At the beginning, the sample is in a single phase; thus it shows no identifiable structure. After 150 s, liquid–liquid phase separation probably occurs, exhibiting some modulated biphasic structures (domains). The domains grow slightly in early time, but they virtually cease to grow further. The cessation of domain growth at long times may be attributed to gelation of the rigid-rod polymer rich solution. The temperature quench to 40 °C reveals a similar trend.

The polarized optical micrographs of Figure 6 show the structure evolution of 8 wt % of BPDA–PFMB/*m*-cresol following a *T* quench to 55 °C. The optical micrograph taken at 6 min exhibits a totally dark appearance indicative of an isotropic phase. After 8 min, some birefringent

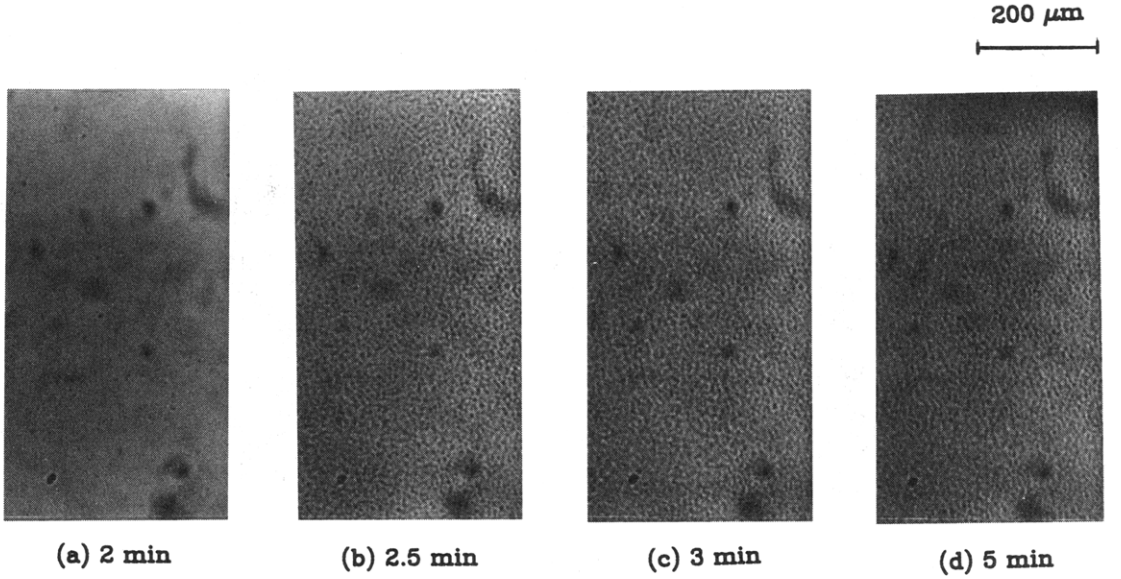

Figure 5. Optical micrographs of the 8 wt % BPDA–PFMB/*m*-cresol solution, displaying interconnected structure. The specimen was first kept at 180 °C for 1.5 min and then quenched to 23 °C for various times.

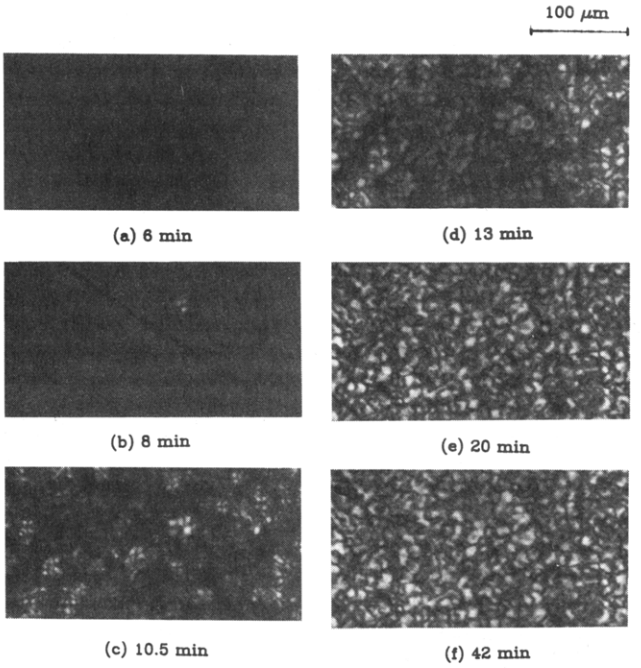

Figure 6. Polarized optical micrographs of the 8 wt % BPDA–PFMB/*m*-cresol solution, showing time evolution of a schlieren texture. The specimen was first kept at 180 °C for 1.5 min and then quenched to 55 °C for various times.

entities develop, which may be associated with liquid crystal defects known as disclinations. These structures are commonly called schlieren textures.[20,21] Concurrently, a continuum of birefringent texture can be discerned in the optical microscope over the entire field of view. The size parameter characterizing the length scale of disclinations will hereafter be referred to as the "domain size". The average domain size increases slightly with time, although it is extremely difficult to quantify from these micrographs. A detailed study of the growth of the liquid crystal domains as observed by time-resolved light scattering will be presented in a later section.

The dependence of disclination textures of BPDA–PFMB/*m*-cresol as a function of quench depth was examined by polarized optical microscopy. The T quenches induced the formation of liquid crystal defects. The average domain size of schlieren textures increases for some initial periods and then levels off. No appreciable change of the structure or the size was noticed after 24 h. Figure 7 shows optical micrographs of 8 wt % BPDA–PFMB/*m*-cresol obtained after 24 h of aging following T quenches from 180 °C to the indicated temperatures. The T quenches to 40, 55, 65, and 75 °C show typical schlieren textures with varying length scales. However, the texture at the T quench to 25 °C appears, although by no means conclusive, somewhat different from the typical schlieren texture. That is, the dark regions are along the polarizer and analyzer directions; thus the structure rather resembles the typical spherulitic morphology of solid crystals. It should be pointed out on the basis of the DSC and light scattering studies that the room temperature is appreciably lower than the monotectic transition (60 °C) that represents the transformation of the ordered rod aggregates to the nematic mesophase. Hence, the rod aggregates may be formed during quenching to ambient temperature. The length scale of the schlieren textures appears to depend strongly on the quenching temperature; namely, the larger the quench depth (ΔT) is, the smaller the average domain size. This behavior will be explored quantitatively by using time-resolved light scattering in a subsequent section.

Kinetic Aspects of Phase Transition. Figure 8 shows light scattering pictures for 8 wt % BPDA–PFMB/*m*-cresol following a T quench from 180 to 23 °C. A four-lobe clover pattern is evident in the Hv scattering, whereas an elongated anisotropic pattern is seen in the Vv configuration. A diffuse scattering halo was observed when polarizers were not utilized. Figure 9 shows the Hv and Vv scattering patterns of the 8 wt % BPDA–PFMB/*m*-cresol solution after quenching from 180 to 75 and 25 °C, respectively. The scattering patterns appear at a lower angle for the T quench at 75 °C relative to that at 25 °C. That is, the average domain size within the sample is larger for the smaller quench depth. This conclusion is consistent with the previous observation by polarized optical microscopy.

Figure 10 illustrates the Vv light scattering patterns evolving in time following the T quench from 180 to 23 °C for 8 wt % BPDA–PFMB/*m*-cresol. Initially, the specimen is in an isotropic state. As time elapses, a diffuse scattering pattern appears, and then the shape becomes anisotropic. The change of the Vv pattern from a circular to an anisotropic shape has been commonly observed during

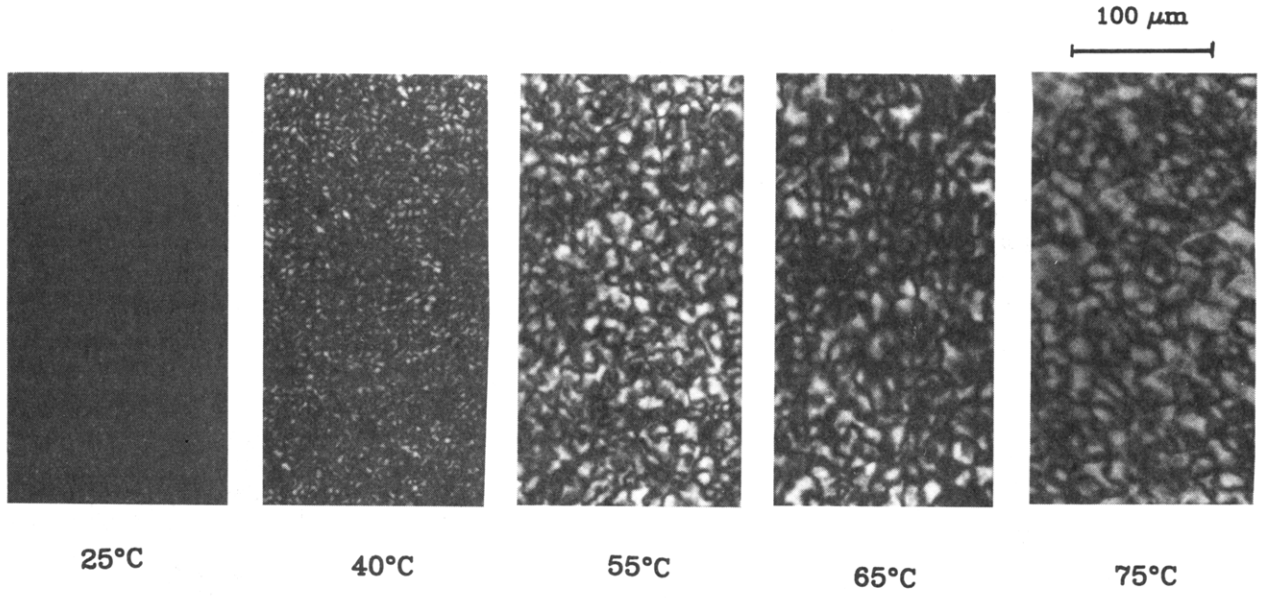

Figure 7. Dependence of schlieren textures on temperature quench depth. The 8 wt % BPDA–PFMB/*m*-cresol solution was first kept at 180 °C for 1.5 min and then quenched to various temperatures.

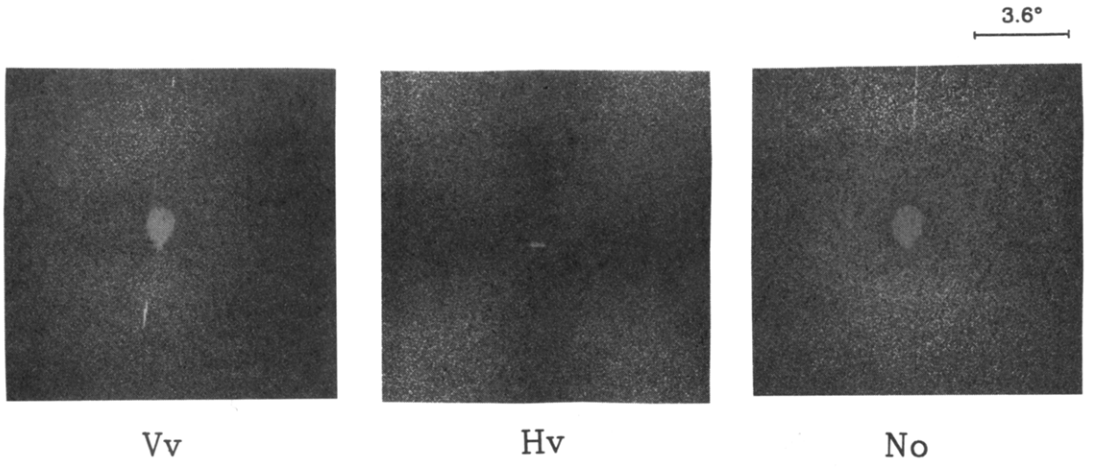

Figure 8. Small-angle light scattering patterns under Vv, Hv, and no polar conditions for the 8 wt % BPDA–PFMB/*m*-cresol solution after a *T* quench to 23 °C.

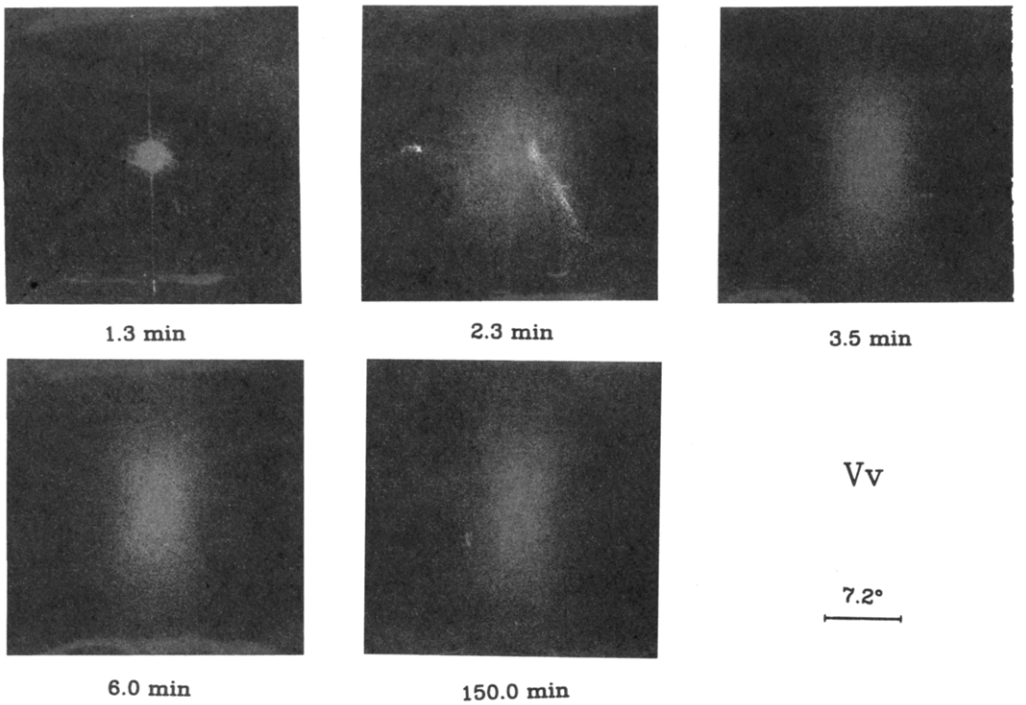

Figure 9. Evolution of the small-angle light scattering Vv patterns with time for the 8 wt % BPDA–PFMB/*m*-cresol solution after a *T* quench to 23 °C.

crystallization from polymeric melts and is generally attributed to the impingement of rod aggregates or domains.[22] The continuum of highly congested schlieren structures may have similar characteristics of impinged rod aggregates. Hashimoto et al.[23] showed that the nematic line disclinations with a strength of ±1 revealed a four-lobe "x" pattern while that with a strength of $\pm^1/_2$ exhibited a rotated four-lobe "+" pattern in the Hv configuration.

Since the time evolution of Vv scattering is complex, the kinetics of phase transition of the BPDA–PFMB/*m*-cresol system was examined solely under the Hv configuration to mimic the growth of domains or the length scale of disclinations. A series of *T* quench experiments were carried out from 180 to 23, 40, 50, and 55 °C. Figures 11 and 12 exhibit the time evolution of scattering peaks of 8 wt % BPDA–PFMB/*m*-cresol at 23 and 55 °C, respectively. The Hv scattering intensity was scanned at an azimuthal angle of 45 °C. The plot of scattering intensity vs scattering wavenumber q shows a maximum corresponding to the periodic distance of neighboring domains. The domain size is larger at the 55 °C quench relative to the *T* quench at 23 °C. Later, these domains impinged on each other; thus the average periodic distance will be equivalent to the average diameter of the domains. As the domain grows, the scattering peak shifts to a lower angle and its intensity increases. Subsequently, the scattering peak becomes stationary, but the intensity continues to increase gradually. The invariance of peak position may be a consequence of the impingement effect. However, there must be a secondary reorganization process such as refinement of internal structure occurring within the preformed domains, thereby causing the scattered intensity to increase.

Figure 13 depicts the logarithmic plot of the growth curves for 8 wt % BPDA–PFMB/*m*-cresol for various temperatures. The domains show two-stage growth. In the first region, the average domain size increases with time in association with the primary transition. The second stage corresponds to the region where the average diameter of the domains shows little or no change in time due to the impingement effect in which the secondary transition takes place internally. The initial slope of the $\log(1/q_{max})$ vs $\log t$ plot yields, except for the 55 °C case, a kinetic growth exponent of approximately 1 for the 23,

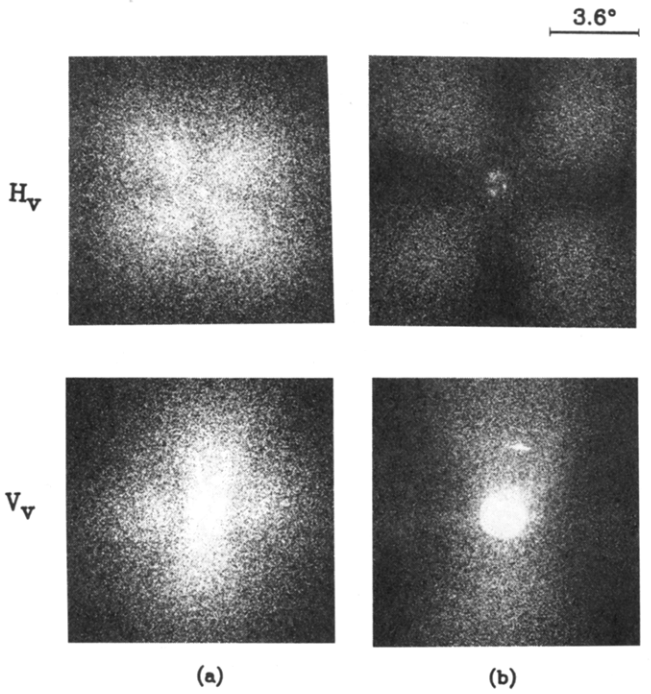

Figure 10. Vv and Hv scattering patterns for the 8 wt % BPDA–PFMB/*m*-cresol solution following a *T* quench at (a) 25 and (b) 75 °C.

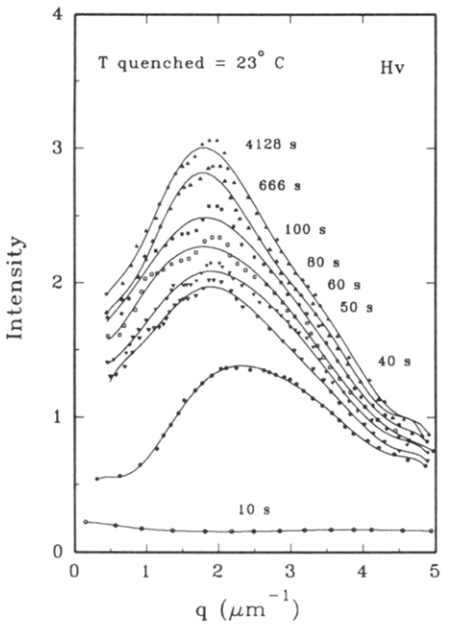

Figure 11. Time evolution of the Hv scattering profile of the 8 wt % BPDA–PFMB/*m*-cresol solution at a *T* quench to 23 °C.

40, and 50 °C quenches. In view of the short time interval at which the slopes were determined, these exponents should not be assigned to any significant mechanisms.

The kinetically equilibrated length scale of orientation fluctuations, i.e., the average domain size, r^*, may be estimated from the Hv light scattering of three-dimensional anisotropic rod aggregates as follows:[23]

$$r^* \frac{4\pi}{\lambda} \sin\left(\frac{\theta_{max}}{2}\right) = 4.1 \quad (1)$$

The ultimate average domain size was found to be the smallest for the lowest *T* quench and increases with increasing quench temperatures or shallower quench depths. To correlate the average domain size to the supercooling ΔT, the classical nucleation theory[24–26] may be adopted by taking into consideration the free energy

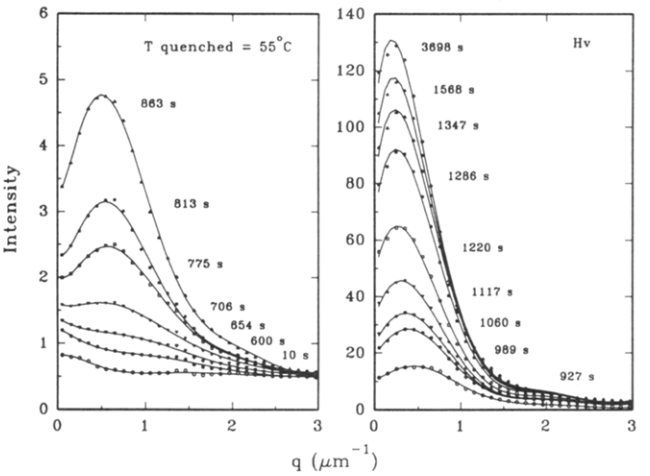

Figure 12. Time evolution of the Hv scattering profile of the 8 wt % BPDA–PFMB/*m*-cresol solution at a *T* quench to 55 °C.

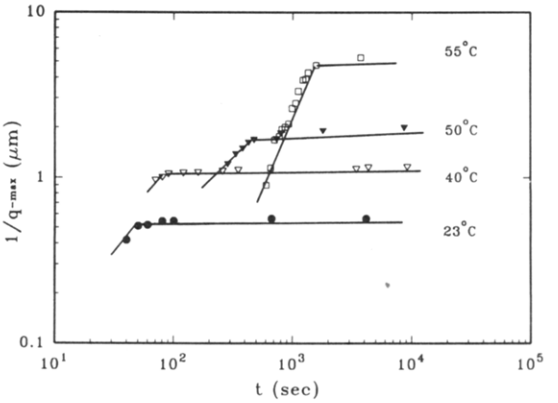

Figure 13. log–log plot of length scale ($1/q_m$) vs time for the 8 wt % BPDA–PFMB/*m*-cresol solution at various temperatures.

change due to the aggregate formation and the associated surface free energy to give

$$r^* = \frac{2\sigma_s}{\Delta H} \frac{T_m}{\Delta T} \quad (2)$$

where σ_s is defined as the surface free energy per cm^2 and ΔH stands for the enthalpy difference per cm^3 between the isotropic and anisotropic phases. Figure 14 shows the linear relationship between the reciprocal critical domain size $1/r^*$ and $\Delta T/T_m$. A slope of 0.454×10^4 ($=\Delta H/2\sigma_s$) was estimated. Using the ΔH value determined by DSC (Figure 1), a surface free energy σ_s of 160.4 erg/cm^2 was estimated. This value is rather large relative to the σ_s of 5.2 and 12.2 erg/cm^2 reported for poly(chlorotrifluoroethylene) (PCTFE) and polyethylene (PE).[27] It may be concluded that the rigid BPDA–PFMB polyimide has a relatively high surface free energy.

Next we examined the kinetic behavior by analyzing the scattering invariant rather than the length scale because the invariant approach will not be affected by the impingement problem. Customarily, the kinetics of domain growth may be interpreted in the framework of the classical nucleation and growth (NG) theory.[24–26] For a three-dimensional domain growth from heterogeneous nuclei, it may be expressed as follows:

$$V_s = 1 - \exp[(-4/3)\pi\nu G^3 t^3] \quad (3)$$

where *G* is the growth rate and ν is the number of nuclei per cm^3. For the nucleation controlled phase transition, the time dependence of ordered rod aggregate fraction

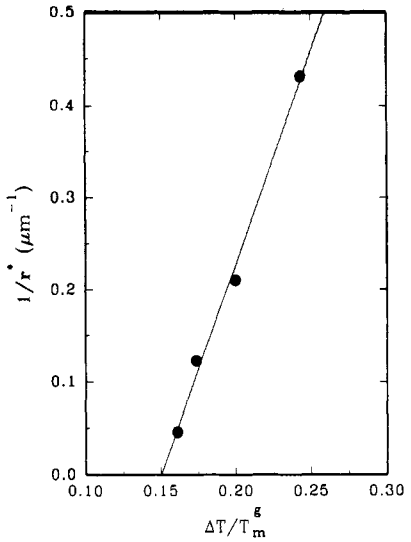

Figure 14. Reciprocal of critical domain size ($1/r^*$) as a function of $\Delta T/T_m^g$ for the 8 wt % BPDA–PFMB/*m*-cresol solution.

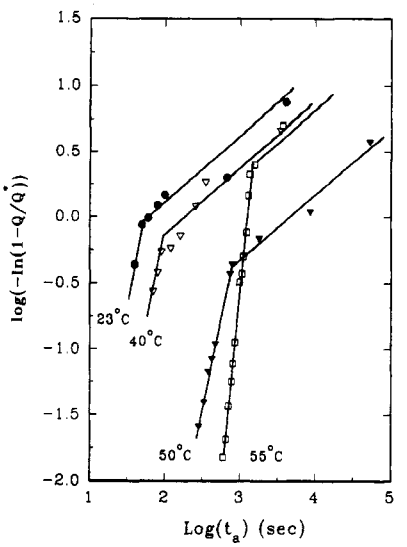

Figure 15. Plot of $\log(-\ln(1 - Q/Q^*))$ vs $\log t_a$ for the 8 wt % BPDA–PFMB/*m*-cresol solution at various temperatures.

$X(t)$ may be expressed in terms of the Avrami equation[24]

$$X(t) = 1 - \exp(-kt^n) \tag{4}$$

where n is the Avrami exponent and k is a constant.

To follow the growth kinetics experimentally, the invariant function of the small-angle light scattering has been customarily employed, which may be determined by integrating the scattered intensity over all scattering volume. The invariant Q for an isotropic system may be expressed in reciprocal space as follows:[28]

$$Q = \int \mathcal{R}(q) q^2 \, dq \tag{5}$$

where $\mathcal{R}(q)$ represents the Rayleigh ratio. The light scattering from semicrystalline or liquid crystalline materials includes contributions from density and orientation fluctuations.[23,29] These contributions may be separated through the depolarized light scattering geometry. Under the Hv scattering, only the contribution from orientation fluctuation is significant, whereas the Vv scattering represents a measure of the combined contributions of density and orientation fluctuations. In the case of random orientation correlation, the scattering invariant due to the contribution of orientation fluctuation Q_{orient} and density fluctuation Q_{dens} may be formulated as[29]

$$Q_{orient} = \int \mathcal{R}(q)_{Hv} q^2 \, dq \sim \langle \delta^2 \rangle \tag{6}$$

$$Q_{dens} = \int \left[\mathcal{R}(q)_{Vv} - \frac{4}{3} \mathcal{R}(q)_{Hv} \right] q^2 \, dq \sim \langle \eta^2 \rangle \tag{7}$$

where $\langle \delta^2 \rangle$ is the mean-square anisotropy fluctuation and $\langle \eta^2 \rangle$ is the mean-square polarizability fluctuation. Based on an ideal two-phase model, Q_{orient} is proportional to the mean-square anisotropy $\langle \delta^2 \rangle$, which is related to the ordered domains when the aggregates are volume-filled, i.e., fully congested ($\langle \eta^2 \rangle = 0$).[21] If the mean-square polarizability $\langle \eta^2 \rangle$ has a nonzero finite value, $\langle \delta^2 \rangle$ is no longer equivalent to the bulk property because the microscopic degree of ordered rod aggregate fraction is no longer constant, but it fluctuates over distances comparable with the wavelength of light. However, the tendency of the relative change of $\langle \delta^2 \rangle$ should be analogous to that of the ordered rod aggregates.

The time dependence of the scattering invariant, Q_{orient}, following various T quench experiments was investigated for the 8 wt % specimen. This scattering invariant Q was calculated by integrating the area under the curve according to eq 5. Figure 15 presents a plot of $\log(-\ln(1 - Q/Q^*))$ vs $\log t_a$ for 8 wt % BPDA–PFMB/*m*-cresol at various temperatures. The double-logarithmic plots of scattering invariant vs time show a two-stage growth behavior. In the first stage, the kinetic exponent is approximately 4 at most quench temperatures, except for the 55 °C quench in which the value is closer to 6. In the second stage, the exponent changes to a value of 0.5 at all quenches. Incidentally, the exponents of 4 and 6 of the first stage correspond to the predicted values for the homogeneous nucleation (three-dimensional growth) of the solid crystal and the solid sheaf (disordered spherulite), respectively.[26] However, it is by no means a proof as the initial slopes cover only a short time scale. Physically, it may be interpreted as the rod molecules self-align and subsequently form bundles as the local concentration of rods increases within the polymer-rich region. These bundles probably act like nuclei upon which the aggregate structures grow until they impinge on each other.

When the impingement of rod aggregate domains takes place, the length scale can no longer increase. However, the refinement of structure or rod alignment would continue internally within the preformed domains. This structural refinement would lead to increased depolarized scattering. Such an internal reorganization of rod aggregates may be attributed to a secondary nucleation and growth process for which the kinetic exponent of 0.5 has been predicted[25,26] and also experimentally observed here.

Conclusions

A partial phase diagram involving liquid–liquid phase separation and the gel–sol transition of the BPDA–PFMB/*m*-cresol system was established by DSC, SALS, and polarized optical microscopy. The gelation in this system is a two-stage process, like many other reversible gels. In the first stage, the rods coalesce into bundles due to an entropic effect. These rod bundles act like physical junctions upon which the aggregate structure grows. In the second stage, the aggregate domains impinge on each other and the refinement of structure or rod alignment probably takes place within the preformed domains.

Above the monotectic transition temperature, the morphology of the BPDA–PFMB/*m*-cresol solution resembles the schlieren textures; but it appears like a solid rod aggregate at the T quench to ambient temperature. The aggregation of rigid-rod polyimides probably takes

place via the nucleation and growth process. The refinement of rod alignment within the preformed aggregates may be attributed to secondary NG, in which the kinetic exponent of 0.5 was obtained for 8 wt % BPDA-PFMB/*m*-cresol. The kinetically equilibrated length scale of rod aggregates was found to be inversely proportional to the quenched depth.

Acknowledgment. The authors acknowledge the National Science Foundation for support provided to the Science and Technology Center for Advanced Liquid Crystal Optical Materials (Grant DMR 89-20147). We thank Professor R. S. Stein for helpful suggestions.

References and Notes

(1) Hwang, W. F.; Wiff, D. R.; Benner, C. L.; Helminiak, T. E. *J. Macromol. Sci., Phys.* **1983**, *22B*, 231.
(2) Russo, P.; Miller, W. G. *Macromolecules* **1983**, *16*, 1690; **1984**, *17*, 1324.
(3) Russo, P. S. *Reversible Polymer Gels and Related Systems*; ACS Symposium Series 350; American Chemical Society: Washington, DC, 1988.
(4) Russo, P.; Chowdhury, A. H.; Mustafa, M. *Mater. Res. Soc. Symp. Proc.* **1989**, *134*, 207. Chowdhury, A. H.; Russo, P. *J. Chem. Phys.* **1992**.
(5) Werbowyj, R. S.; Gray, D. G. *Macromolecules* **1980**, *13*, 69.
(6) Kyu, T.; Mukherjee, P. *Liq. Cryst.* **1988**, *3* (5), 631. Kyu, T.; Zhuang, P.; Mukherjee, P. *Polymer Association Structures: Microemulsions and Liquid Crystals*; El-Nokaly, M. A., Ed.; ACS Symposium Series 384; American Chemical Society: Washington, DC, 1989; Chapter 16.
(7) Flory, P. J. *Proc. R. Soc. London* **1956**, *234A*, 73.
(8) Doi, M.; Shimada, T.; Okano, K. *J. Chem. Phys.* **1988**, *88*, 4070.
(9) Khokhlov, A. R.; Semenov, A. N. *J. Stat. Phys.* **1985**, *38*, 161.
(10) Harris, F. W.; Hsu, S. L.-C. *High Perform. Polym.* **1989**, *1*, 1; *Polym. Prepr. (Am. Chem. Soc., Div. Polym. Chem.)* **1989**, *30*, 187; **1990**, *31*, 342.
(11) Cheng, S. Z. D.; Wu, Z.; Eashoo, M.; Hsu, S. L.-C.; Harris, F. W. *Polymer* **1991**, *32*, 1803. Harris, F. W. *Ibid. Macromolecules* **1991**, *24*, 1983.
(12) Fukai, T.; Yang, J. C.; Kyu, T.; Cheng, S. Z. D.; Lee, S. K.; Hsu, S. L.-C.; Harris, F. W. *Polymer* **1992**, *33*, 3621.
(13) Pennings, A. J. *J. Polym. Sci., Polym. Symp.* **1977**, *59*, 55; Kalb, B.; Pennings, A. J. *Polymer* **1980**, *21*, 3.
(14) Smith, P.; Lemstra, P. J. *Macromol. Chem.* **1979**, *180*, 2983; *J. Mater. Sci.* **1980**, *15*, 505.
(15) Sawatari, C.; Okumura, T.; Matsuo, M. *Polym. J.* **1986**, *18*, 741.
(16) Lee, S. K.; Cheng, S. Z. D.; Wu, Z. Q.; Lee, C. J.; Kyu, T.; Yang, J. C. *Polym. Int.* **1993**, *30*, 115.
(17) Mutin, P. H.; Guenet, J. M. *Macromolecules* **1989**, *22*, 843.
(18) Komatsu, M.; Inoue, T.; Miyasaka, K. *J. Polym. Sci., Polym. Phys. Ed.* **1986**, *24*, 303.
(19) Coniglio, A.; Stanley, H. E.; Klein, W. *Phys. Rev. Lett.* **1979**, *42*, 518.
(20) Glotzer, S. C.; Sciortino, F.; Gyure, M.; Bansil, R.; Stanley, H. E. *Bull. Am. Phys. Soc.* **1992**, I34, 16; *Nature*, submitted.
(21) Rojstaczer, S. R.; Stein, R. S. *Macromolecules* **1990**, *23* (22), 4863.
(22) Shiwaku, T.; Nakai, A.; Hasegawa, H.; Hashimoto, T. *Macromolecules* **1990**, *23* (6), 1590.
(23) Stein, R. S.; Rhodes, M. B. *J. Appl. Phys.* **1960**, *31*, 1873.
(24) Avrami, M. *J. Chem. Phys.* **1941**, *9*, 177.
(25) Mandelkern, L. *Crystallization of Polymers*; McGraw-Hill: New York, 1964.
(26) Wunderlich, B. *Macromolecular Physics, Crystal Nucleation, Growth, Annealing*; Academic Press: New York, 1976; Vol. 2.
(27) Hoffman, J. D.; Weeks, J. J. *J. Chem. Phys.* **1962**, *37* (8), 1723.
(28) Higgins, J. S.; Stein, R. S. *J. Appl. Crystallogr.* **1978**, *11*, 346.
(29) Koberstein, J.; Russell, T. P.; Stein, R. S. *J. Polym. Sci., Polym. Phys. Ed.* **1979**, *17*, 1719.